J Neurophysiol 101: 491–502, 2009.
First published November 12, 2008; doi:10.1152/jn.90335.2008.

Methods for Determining Frequency- and Region-Dependent Relationships Between Estimated LFPs and BOLD Responses in Humans

Roberto Martuzzi,[1–3] Micah M. Murray,[1,3,4] Reto A. Meuli,[1,3] Jean-Philippe Thiran,[2,3] Philippe P. Maeder,[1,3] Christoph M. Michel,[3,5] Rolando Grave de Peralta Menendez,[6,7] and Sara L. Gonzalez Andino[6]

[1]*Radiology Service and* [4]*Neuropsychology and Neurorehabilitation Service, University Hospital Center and University of Lausanne, Lausanne, Switzerland;* [2]*Signal Processing Institute, Ecole Polytechnique Fédérale de Lausanne, Lausanne, Switzerland;* [3]*Center for Biomedical Imaging of Lausanne and Geneva, Lausanne, Switzerland;* [5]*Functional Brain Mapping Laboratory and* [6]*Electrical Neuroimaging Group, Department of Neurology, University Hospital, Geneva, Switzerland; and* [7]*Neurodynamics Laboratory, Department of Psychiatry and Clinic Psychobiology, University of Barcelona, Catalonia, Spain*

Submitted 6 March 2008; accepted in final form 9 September 2008

Martuzzi R, Murray MM, Meuli RA, Thiran JP, Maeder PP, Michel CM, Grave de Peralta Menedez R, Gonzalez Andino SL. Methods for determining frequency- and region-dependent relationships between estimated LFPs and BOLD responses in humans. *J Neurophysiol* 101: 491–502, 2009. First published November 12, 2008; doi:10.1152/jn.90335.2008. The relationship between electrophysiological and functional magnetic resonance imaging (fMRI) signals remains poorly understood. To date, studies have required invasive methods and have been limited to single functional regions and thus cannot account for possible variations across brain regions. Here we present a method that uses fMRI data and singe-trial electroencephalography (EEG) analyses to assess the spatial and spectral dependencies between the blood-oxygenation-level-dependent (BOLD) responses and the noninvasively estimated local field potentials (eLFPs) over a wide range of frequencies (0–256 Hz) throughout the entire brain volume. This method was applied in a study where human subjects completed separate fMRI and EEG sessions while performing a passive visual task. Intracranial LFPs were estimated from the scalp-recorded data using the ELECTRA source model. We compared statistical images from BOLD signals with statistical images of each frequency of the eLFPs. In agreement with previous studies in animals, we found a significant correspondence between LFP and BOLD statistical images in the gamma band (44–78 Hz) within primary visual cortices. In addition, significant correspondence was observed at low frequencies (<14 Hz) and also at very high frequencies (>100 Hz). Effects within extrastriate visual areas showed a different correspondence that not only included those frequency ranges observed in primary cortices but also additional frequencies. Results therefore suggest that the relationship between electrophysiological and hemodynamic signals thus might vary both as a function of frequency and anatomical region.

INTRODUCTION

Despite the widespread use of hemodynamic imaging methods in neuroscience, the relationship between blood-oxygen-level-dependent (BOLD) and electrophysiological signals remains controversial. It is unclear whether the BOLD signal corresponds to action potentials (Heeger et al. 2000; Rees et al. 2000), specific frequency bands of postsynaptic activity as measured by local field potentials (LFPs) (Kayser et al. 2004; Niessing et al. 2005; see also Mathiesen et al., 2000), or both multi-unit activity (MUA) and LFPs (Logothetis 2003; Logothetis et al. 2001; Mukamel et al. 2005). Moreover, studies have hitherto been invasive and limited to single brain regions rather than the entire brain volume.

Even when correlations with BOLD signals are observed for both MUA and LFPs, the latter has consistently exhibited a stronger relationship. LFPs are a prime candidate for correspondence with BOLD signals because synaptic activity constitutes the bulk of neuronal metabolism (Sibson et al. 1998), and BOLD responses have been observed in the absence of measurable single-unit activity (Gandhi et al. 1999; Blake and Logothetis 2002; Polonsky et al. 2000). Nonetheless, the correlation between BOLD signals and MUA was consistently significant although weaker than that with LFP (e.g., Logothetis et al. 2001). Thus the role of MUA cannot be entirely discounted. Additionally, very high-frequency oscillations (VHFOs) within the LFP appear to be more tightly linked to MUA than to LFP oscillations in lower frequency bands (Kreiman et al. 2006), raising the possibility that VHFOs in surface-recorded EEG in humans might provide insights into a wider range of neuronal activity (e.g., Gonzalez et al. 2006). To date, noninvasive studies in humans have assessed the spatial correspondence between BOLD responses and source estimations from surface-recorded event-related potentials (ERPs) (e.g., Dale and Halgren 2001) and steady-state visual evoked potentials (SSVEPs) (Di Russo et al. 2007), although these assessments were always qualitative rather than quantitative in nature.

It is further likely that regional anatomy influences the shape of the BOLD signal and therefore its correspondence to neural activity, which in turn would result in variation in neurovascular coupling throughout the brain (Logothetis and Wandell 2004). This variation, in conjunction with the aforementioned discrepancies regarding which neurophysiologic signal(s) best correspond with the BOLD response, highlights the imperative for methods that noninvasively measure electrical signals throughout the brain volume while also retaining sensitivity to high frequencies.

Present address and address for reprint requests and other correspondence: R. Martuzzi, Dept. of Diagnostic Radiology, Yale School of Medicine, The Anlyan Center, 300 Cedar Street, TAC-N134, P.O. Box 208042, New Haven, CT 06519 (E-mail: roberto.martuzzi@yale.edu); S. L. Gonzalez Andino, Electrical Neuroimaging Group, Department of Neurology, University Hospital, 24 rue Micheli-du-Crest, 1211 Geneva, Switzerland (E-mail: sara.gonzalezandino@hcuge.ch).

The costs of publication of this article were defrayed in part by the payment of page charges. The article must therefore be hereby marked "*advertisement*" in accordance with 18 U.S.C. Section 1734 solely to indicate this fact.

Here we compare BOLD and electrical signals acquired noninvasively during two separate sessions from the same healthy participants. We then estimated intracranial LFPs (eLFP) within the whole brain volume (Grave de Peralta Menendez et al. 2000, 2004) to explore the spatial and spectral dependencies between these signals. Comparable activation maps from both the EEG and fMRI data sets were obtained, without losing sensitivity to high-frequency oscillations, through the analysis of single-trial spectral power. We demonstrate, using a visual stimulation paradigm, that the relationship between eLFP and BOLD signals varies across frequencies and regions.

METHODS

EEG single-trial analysis

We developed an analysis method for the statistical comparison of the spectral power between the pre- and poststimulus periods computed for each single trial to preserve the high-frequency information of the EEG signals. This analysis was conducted on the eLFPs (Grave de Peralta Menendez et al. 2000, 2004; see following text for further details).

The processing steps of the single-trial analysis are schematized in Fig. 1. After artifact rejection and interpolation of bad channels, each single trial was isolated including the same number of samples in the pre- and poststimulus onset periods. The inverse solution for each single trial was then separately estimated. For each of these inverse estimates, we computed the power spectrum in the pre- and in the poststimulus onset periods. Because these two periods had the same duration (in this study 500 ms each), the spectral resolution of the two power spectrum densities had the same frequency resolution (i.e., 2 Hz). The power spectrum was computed over the selected pre- and poststimulus periods using a multi-taper method with seven Slepian data tapers (Thomson 1982). This method minimizes the variance of the estimates; this is important when quantifying VHFOs the amplitude of which is often below the noise level and for time series with a large dynamic range as the ones considered here. For the duration considered here, we used an 8-Hz bandwidth parameter. The variance was reduced sevenfold by using seven Slepian data tapers. Each 500-ms time period was multiplied by each of the tapers, and the Fourier components were then computed via fast Fourier transform (FFT). The power spectral density was then computed by taking the square of the modulus of the FFT from 0 to 256 Hz (i.e., half of the frequency sampling). Given N single trials for an individual subject, we obtained N estimates of the spectral power during the prestimulus onset period and N estimates for the poststimulus onset period that were then statistically compared. In this way, we statistically identified the positions and frequencies showing spectral power changes in response to stimulus onset. Nonparametric statistical comparisons were performed using the sign test, which in turn generated 128 statistical maps (i.e., 1 per frequency bin from 0–256 Hz, at steps of 2 Hz). Our analyses assume that noise is equally distributed across both pre- and poststimulus onset periods, which means that noise does not contribute to stimulus-linked power changes. Because no signal averaging is performed, this method can detect power changes even at very high frequencies, where the noise is typically much higher than the signal.

For each subject, we then estimated the median of the power spectral difference between the pre- and poststimulus periods and these estimates (1 per subject) were then submitted to the nonparametric sign test to assess whether these estimates come from a population with zero median (voxel-level threshold $P < 0.01$ uncorrected, 3-voxel cluster-size threshold). Inference on the population was obtained using a second level of statistics, using the same threshold as for individual-subject analyses.

Comparison between fMRI and EEG results

The analyses of the fMRI and EEG data yielded two different sets of statistical maps representing stimulus-driven brain activations. There are many details to consider in the quantitative comparison of these statistical maps. First, there can be a certain level of error in the localization of the eLFPs and, by extension, their spectral power

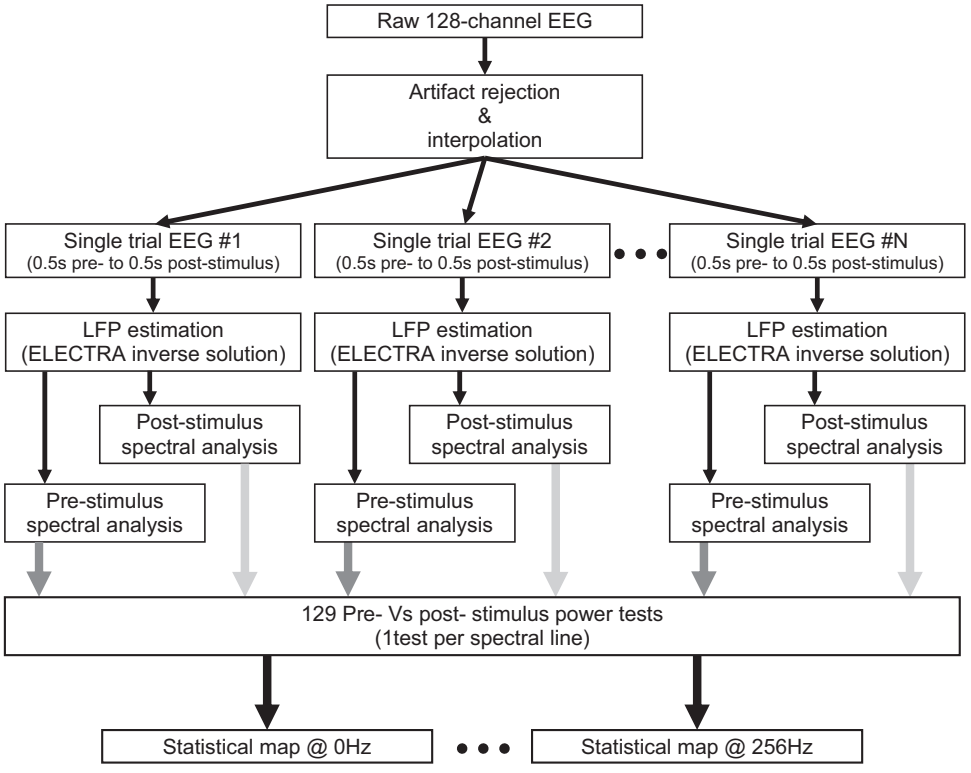

FIG. 1. Schematic representation of the single-trial analysis for the electroencephalographic (EEG) dataset.

changes. Similarly, fMRI results can be slightly displaced with respect to the actual active areas. Consequently, even small misalignment of the fMRI results and of the eLFPs can produce high underestimation of their spatial correlation using a strict voxel-wise approach. We therefore conducted region-wise instead of voxel-wise analyses. Moreover, there is no a priori hypothesis supporting the idea that the neurovascular coupling is constant across brain regions. For these two reasons, we separated the different Brodmann areas (BA) of the brain and computed the comparison between EEG and fMRI within each area, separately.

The metric used to compute the *resemblance index* (RI) of the activation maps for each region r and frequency f is defined as

$$\text{resemblance}(r,f) = 1 - \frac{|m_{r,\text{LFP}}(f) - m_{r,\text{fMRI}}|}{|m_{r,\text{LFP}}(f) + m_{r,\text{fMRI}}|}$$

where $m_{r,\text{LFP}}(f)$ is the number of LFP active voxels within the region r at the frequency f divided by the total number of LFP active voxels at the frequency f, and $m_{r,\text{fMRI}}$ is the number of fMRI active voxels within the region r divided by the total number of fMRI active voxels. By construction, RI is bounded by 0 and 1, with higher values indicating higher local correspondence between the two statistical maps within that specific region and at that specific frequency.

For each separate region (i.e., BA) we obtained a RI value. Statistical analysis was performed by comparing this value with the empirical distribution estimated for each BA. To compute the empirical distribution, we calculated the RI between the fMRI values of the region and an equal number of LFP values randomly sampled across the brain. An empirical distribution was obtained by iterating this process 100,000 times. Statistics on this metric were calculated on this estimated empirical distribution and thresholded at $P < 0.05$. Recall that the labeling of active voxels within fMRI and each frequency of the LFP was identical ($P < 0.01$ with a 3-voxel cluster-size minimum). As an alternative second level of statistics, within each of the BAs of interest we computed the RI for each subject individually and then applied a sign test to investigate whether these values come from a population with zero median. Because this analysis is based on single-subject results, we applied a more severe threshold ($P < 0.001$ with a 3-voxel cluster-size minimum) for the identification of active voxels in both fMRI and eLFP datasets.

As a complement to the RI analysis, which provides qualitative information on the correspondence between fMRI signals and the different EEG frequencies, we also computed the correlation between the differences in fMRI signal amplitude and EEG spectral power in response to the stimulus onset. To evaluate the correlation across reliable changes in the two signals, this correlation analysis was limited to those frequencies showing a significant change in spectral power between the pre- and poststimulus onset periods.

Experimental data

SUBJECTS AND PARADIGM. Eight subjects (aged 24–39 yr; 4 female; 5 right-handed and 3 left-handed) with normal or corrected-to-normal vision and no history of neurological or psychiatric illnesses participated in this study. Experimental procedures were approved by the Ethics Committee of the Faculty of Biology and Medicine of the University of Lausanne.

Subjects completed separate EEG and fMRI sessions involving identical stimulation. In all cases, except one, the EEG session was completed prior to the fMRI session. The separation between sessions ranged from 2 to 74 days (except in the case where the fMRI session preceded the EEG session by 1 day). Subjects passively viewed a visual stimulus (70° wedge of a black-on-gray circular checkerboard presented to the lower left visual quadrant and flickering at 8 reversals per second) for durations of 12 s followed by 18 s of rest (i.e., fixation point only). The experiment included 42 (fMRI) or 126 (EEG) repetitions of the stimulation block. See Fig. 2*A* for a schematic representation of the stimulus and of the paradigm timeline.

MAGNETIC RESONANCE IMAGING. Functional MRI data were acquired on a 3.0 T Siemens Trio system equipped with an eight-channel head coil using a single-shot gradient-echo EPI sequence (TR = 2 s, TE = 30 ms, FoV = 224 mm, flip angle = 90°, matrix size: 64 × 64). Each volume comprised 32 slices (slice thickness: 3 mm, gap: 0.3 mm). For each subject, a sagittal T1-weighted gradient-echo sequence (MPRAGE) was also acquired (160 contiguous sagittal slices, slice thickness 1 mm, matrix size 256 × 256, TR = 1,480 ms, TE = 3.42 ms, FoV = 256 mm, flip angle = 15°).

Magnetic resonance images were processed with SPM2 (Wellcome Department of Cognitive Neurology, London, UK). Structural data were normalized to the Montreal Neurological Institute (MNI) template and re-sampled to a resolution of 1 ×1 × 1 mm^3. Functional data were first co-registered to the structural volume and spatially realigned to the first image acquired (to minimize effects of head motion during the acquisition) and then normalized to the Montreal Neurological Institute (MNI) template.

Two types of fMRI analyses were conducted. The first analysis was conducted without considering EEG recordings to asses whether visual activations were localized according to retinotopic predictions, which would suggest subject compliance with central fixation. For this analysis, volumes were re-sampled to the resolution of 3 × 3 × 3 mm^3 and smoothed with an isotropic Gaussian kernel (FWHM = 6 mm). The second analysis was conducted to compare fMRI and EEG results. Therefore fMRI data were downsampled to the resolution of the inverse solution grid used in the analysis of EEG data (i.e., 6 ×6 × 6 mm^3) and no additional smoothing was performed, as this was effectively the consequence of the above down-sampling. For both analyses, the temporal signal at each voxel was high-passed filtered to minimize the effect of a baseline drift, and statistical analyses were conducted according to the General Linear Model using as basis function the boxcar representing the experimental protocol convolved with the canonical hemodynamic response function (Friston 1998). Population-level inference (group analysis) was obtained by second-level statistics.

EEG DATA ACQUISITION AND PREPROCESSING. Continuous 128-channel EEG was acquired at 512 Hz (BioSemi Active Two, Amsterdam, The Netherlands). Preprocessing procedures included single-trial selection (from −500 pre- to 500 ms poststimulus onset), artifact rejection (±100 μV artifact rejection criterion in addition to the removal of EEG epochs containing eye blinks or other noise transients), interpolation of signal at artifact electrodes (Perrin et al. 1987), and re-referencing to the common average. For each subject, intracranial LFPs were estimated with the ELECTRA inverse solution. ELECTRA is based on the fact that independent of the volume conductor model used to describe the head, solenoidal currents do not contribute to the EEG, and thus electric measurements are entirely determined by irrotational currents (Grave de Peralta Menendez et al. 2000, 2004). Importantly this is not assumption but a mathematical physics property derived from the quasi-static Maxwell's equations. Furthermore, available experimental evidence in excitable tissues shows that secondary macroscopic currents are several orders of magnitude higher than primary macroscopic currents (Plonsey 1982;). This property yields a new formulation of the inverse problem based on a first kind Fredholm integral equation that relates intracranial LFPs to scalp EEG measurements. While this relationship is theoretically unquestioned it is not sufficient to uniquely determine the LFPs at an unlimited number of brain voxels. Therefore a regularization strategy must be used to select a unique solution. In our case, we used a local autoregressive model (LAURA); which applies the physical principle concerning the spatial relationships between the estimated potentials at neighboring voxels, such that LFPs decay as a function of the square distance to the source. Prior basic and clinical research from our group has documented and discussed in detail the spatial accuracy

of the ELECTRA inverse model (e.g., Gonzalez Andino et al. 2005a,b; Grave de Peralta Menendez et al. 2004; Michel et al. 2004). Importantly, the methodology presented here is based on the estimation of the frequency content associated to each voxel (eLFP's), which in turn depends only on the estimated time courses. Under the quasi-static approximation, no capacitive effects exist in neural tissue. Therefore high and low frequencies (of biological relevance) propagate instantaneously trough the tissue. This has been experimentally confirmed by Logothetis et al. (2007) who found that "the cortical tissue acts as an ohmic conductor that allows the unbiased propagation of any biologically relevant temporal frequency." Therefore frequencies present on the EEG will be transferred by the linear inversion procedure to the eLFP. Further evidence for this aspect comes from recent studies from Murakami et al. (2002, 2003) that aimed to clarify the origins of scalp-recorded magnetic and electric fields and showed that spiking activity, if sufficiently synchronized, might be detectable by scalp recordings in the form of very high-frequency oscillations.

The solution space (i.e., the lead field matrix) was calculated on a realistic head model that included 4024 nodes, selected from a 6 × 6 × 6-mm grid of voxels equally distributed within the gray matter of the MNI's average brain. To fully understand the error in the localization of the eLFP, we must consider two different aspects: *1*) the accuracy in the estimation of the source amplitudes at each voxel; *2*) the resolution, i.e., the smearing in the estimation of the activity linked to a single source. This principle holds for any linear distributed solution, and this problem is much more complex than simply estimating the localization error for all single sources alone. Only a full analysis of the resolution kernels can completely answer these questions because the estimators are, for all linear solutions to underdetermined problems, biased by the presence of simultaneously activated sources. One generalization is that the localization accuracy is variable and decreases as a function of the source eccentricity. For the cortical locations considered here, the localization accuracy is in the order of the grid size (i.e., a few millimeters) and the resolution kernels are correctly centered around the right source location with little interference from distant sources (little blurring).

RESULTS

Figure 2 shows the results of the first fMRI analysis (i.e., at the resolution of 3 × 3 × 3 mm^3) in the glass brain and on slices overlaid on the mean structural volume across subjects. The strongest activations ($P < 0.001$, cluster-size >10 voxels) are located in the upper right bank of the calcarine sulcus and surrounding occipital cortex. This pattern of activations is consistent with retinotopic predictions for a visual stimulus located within the lower left quadrant of the visual field. Additional activations were observed within extrastriate cortices bilaterally.

The results of the second fMRI analysis (i.e., at the resolution of 6 × 6 × 6 mm^3) are shown on axial slices overlaid on the group-average structural volume in Figs. 3*A* and 4*A* and are rendered in a glass brain in Supplementary Fig. S1.[1] Active regions ($P < 0.01$, cluster-size >3 voxels) as defined by fMRI were mainly identified within BA17 of the right hemisphere and BA18/19 bilaterally (see Figs. 3*C* and 4*C* for the definition of BAs), as well as in adjacent areas outside of the occipital lobe (BA7, BA37, and BA40).

Figure 5 illustrates the grand mean of the estimated LFPs at some representative voxels. This is the equivalent to computing the inverse solution on the event-related potential, which will forcibly be predominated by lower frequencies (cf. Tallon-Baudry and Bertrand 1999). First, this analysis shows that the

[1] The online version of this article contains supplemental data.

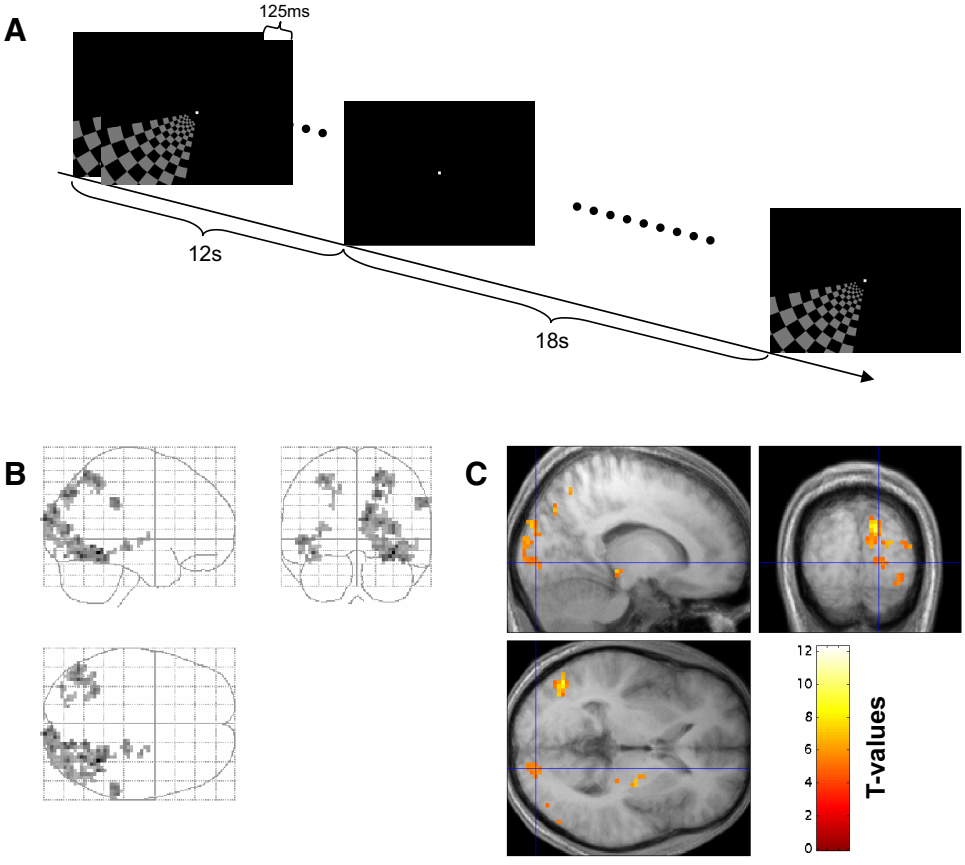

FIG. 2. Stimulation protocol (*A*) and functional mangentic resonance imaging (fMRI) activations ($P < 0.001$; cluster-threshold 10 voxels) in the glass brain (*B*) and on slices overlaid on the mean structural volume across subjects (*C*).

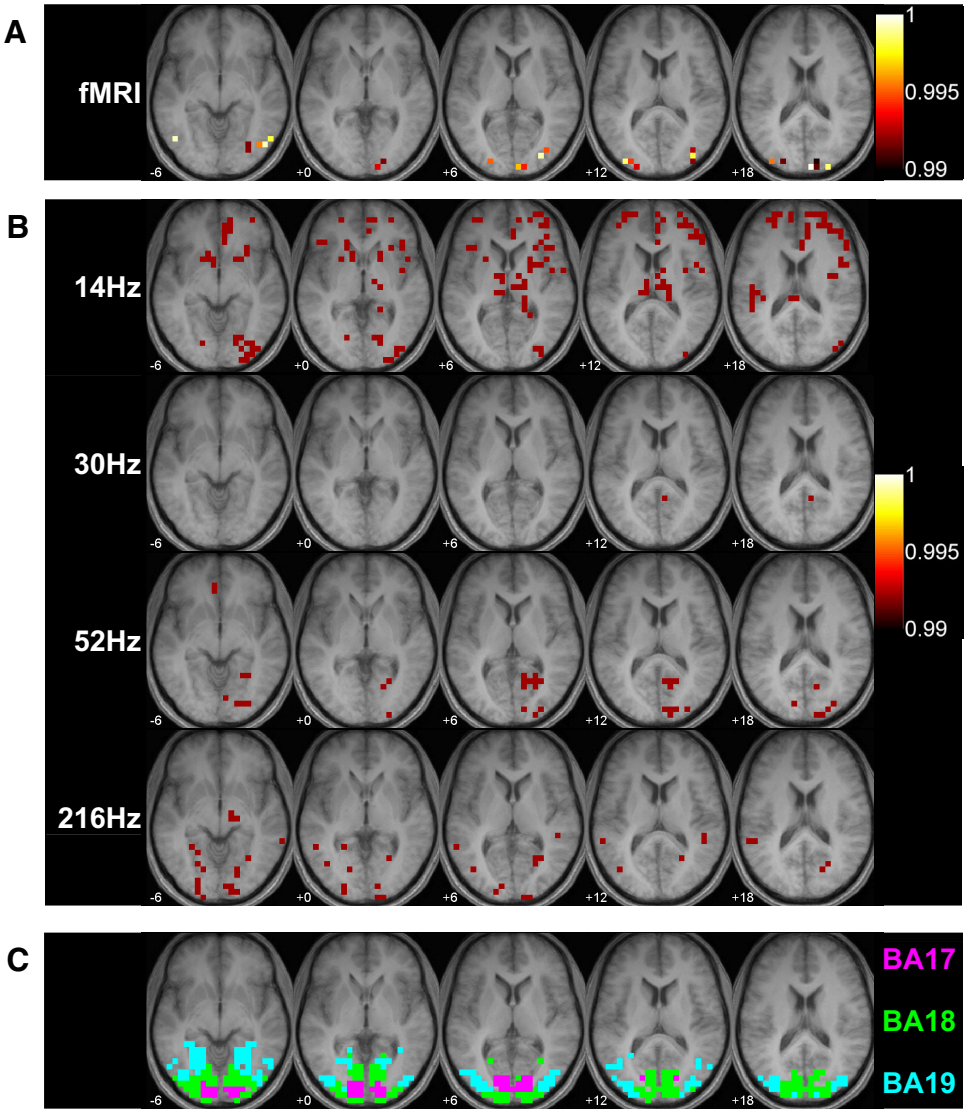

FIG. 3. fMRI and local field potential (LFP) activations within the occipital lobe. *A*: fMRI activations; *B*: exemplar LFP activations at 14, 30, 52, and 216 Hz ($P < 0.01$ uncorrected, cluster-threshold 3 voxels; see RESULTS for details). *C*: illustration of the definition of Brodmann Areas BA17 (magenta), BA18 (green), and BA19 (cyan). Activations are shown on axial slices overlaid on the group-average structural volume.

responses are largely restricted to the visual cortices, and responses within frontal cortices did not differ between pre- and poststimulus onset periods. Second, within the occipital lobe responses are lateralized to the hemisphere contralateral to the visual stimulus (i.e., the right hemisphere). As was the case for the fMRI analyses, this pattern of responses is consistent with retinotopic predictions given our stimulus, suggestive of subjects' compliance with the task also during the EEG recording session. Additional responses were observed within extrastriate cortices bilaterally.

Single-trial LFP analyses show that the spatial distribution of stimulus-driven power spectrum modulations differed as a function of frequency. For example, at 30 Hz, few and relatively sparse voxels showed a change in spectral power between the pre- and poststimulus periods, whereas at lower frequencies (i.e., ≤14 Hz) and higher frequencies (e.g., 52 and 216 Hz), there are power changes in locations similar to those identified by fMRI. Activations at representative frequencies are shown in Figs. 3*B* and 4*B*. Higher frequency responses were largely restricted to parieto-occipital cortices. Lower frequency (e.g., ≤14 Hz) responses extended into frontal cortices, supporting the role for these frequencies and regions in maintaining visuo-spatial attention (e.g., Worden and Foxe 2003). A consequence of this extended pattern is generally lower RI between these frequencies (see following text).

To quantitatively and statistically evaluate the co-localization of LFP and fMRI activations, we computed the RI across frequencies for areas within the occipital lobe (BA17, BA18, and BA19 bilaterally).[2] Results are shown in Fig. 6. Within BA17, nonzero *resemblance* was limited to the right hemisphere (i.e., that contralateral to the stimulus) and was clustered around three frequency bands; low frequencies (≤14 Hz), the gamma band range (44–78 Hz), and VHFOs (>200 Hz). Statistically significant values were observed at 220 Hz, and marginally significant ($0.05 < P < 0.1$) values were observed at 60 Hz. Within BA18, nonzero RI values were bilateral and clustered around the same frequencies in each hemisphere. These frequency clusters not only incorporated those observed within BA17 but also included a wider range of gamma band activity as well as activity at ~170 Hz bilaterally and at 252 Hz within the left hemisphere. Statistically significant values were

[2] Resemblance was also computed for regions adjacent to the occipital lobes that showed activation in the fMRI analysis (see Supplementary Fig. S2).

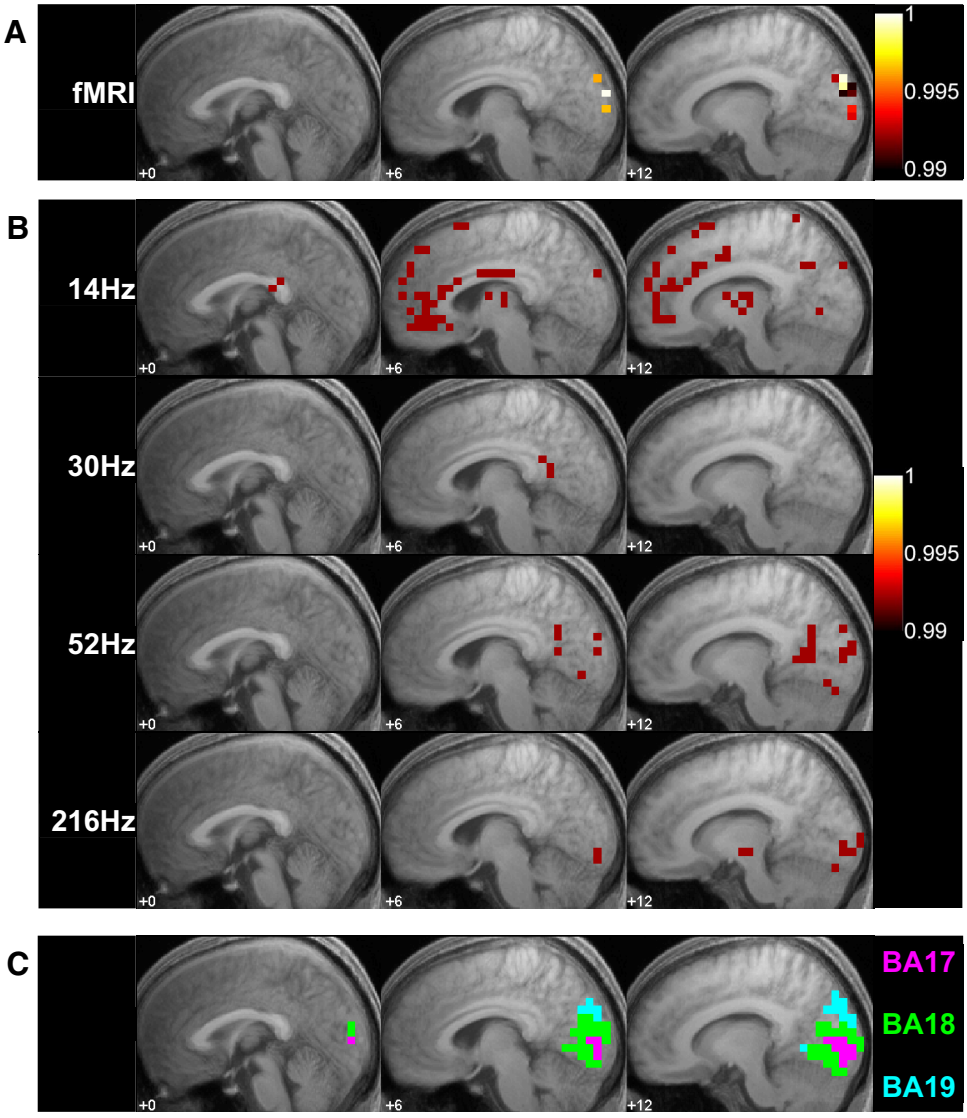

FIG. 4. fMRI and LFP activations within the right hemisphere. *A*: fMRI activations; *B*: exemplar LFP activations at 14, 30, 52, and 216 Hz ($P < 0.01$ uncorrected, cluster-threshold 3 voxels; see RESULTS for details). *C*: definition of Brodmann Areas BA17 (magenta), BA18 (green), and BA19 (cyan). Activations are shown on sagittal slices overlaid on the group-average structural volume.

also more widespread, particularly within the right hemisphere and included all the abovementioned frequency clusters (see Fig. 6). Within left BA18, only the lowest frequency cluster (≤14 Hz) showed significant *resemblance*. Within BA19, nonzero *resemblance* values remained bilateral and were further widespread in their spectral range. In addition, nonzero values were observed at ~90–110 Hz within the right hemisphere and at ~146–156 Hz within the left hemisphere. As was the case for BA18, statistically significant values within BA19 were observed at all of the abovementioned frequencies (see Fig. 6). To test the sensitivity of the RI to the threshold used for identifying active voxels, we repeated the same resemblance analyses with a threshold set at $P < 0.05$ (and 3-voxel cluster-threshold). The results do not noticeably differ from those reported in the preceding text (Supplementary Fig. S3).

Finally, we adopted an alternative method to compute group results. In this approach, the RI for each of the BAs of interest was computed for each individual subject. Then we computed the median of these values and tested whether these values could be drawn from a population with zero mean, using a nonparametric sign test. Median values (Fig. 7) show a frequency- and region-variable pattern similar to that shown by the previous group analysis, but few of these RI values are statistically significant. This issue can be ascribed to the reduced sensitivity of nonparametric tests in conjunction with the relatively small population used in this study.

We also computed the correlation between BOLD signal and eLFP power increase between the pre- and poststimulus onset periods, restricting our analysis to those frequencies exhibiting a nonzero RI. Results are presented in Fig. 8 and show that in BAs 17 and 18 within the hemisphere contralateral to the stimulus, an increase of BOLD signal is associated with an increased the eLFP power in the high gamma band (40–100 Hz) and with decreased eLFP power in the VHFOs. Conversely, within the hemisphere ipsilateral to the stimulus, the BOLD signal increase is associated with a reduced power of the eLFPs in the gamma band. Within BA19, the correlations between BOLD signal and eLFP power changes are weaker than in the two preceding areas. It is worth noting that in the VHFOs, this correlation is no longer valid within the contralateral hemisphere, while it becomes statistically reliable in the hemisphere ipsilateral to the stimulus.

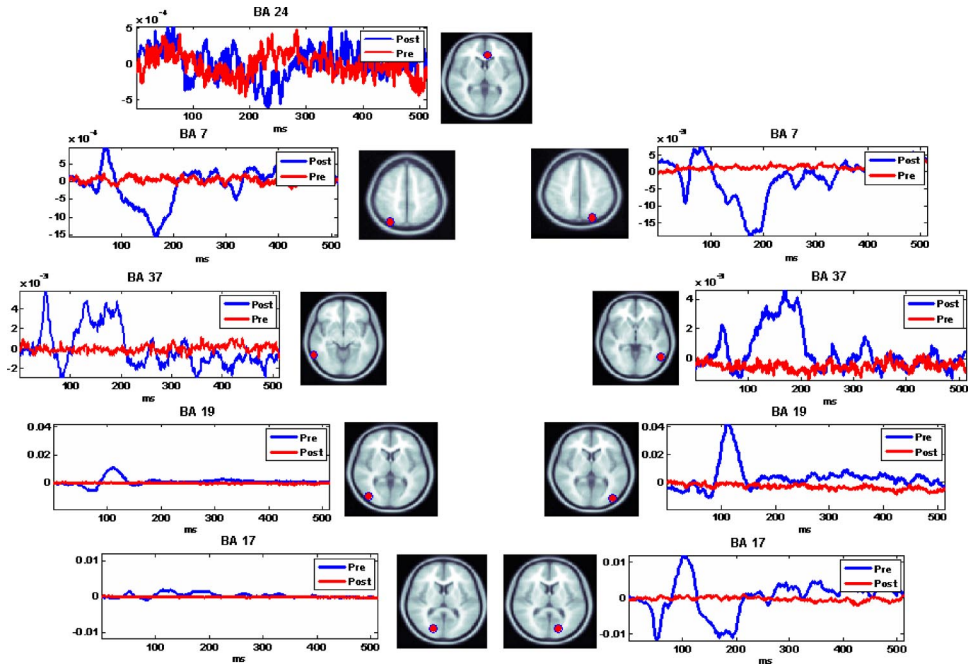

FIG. 5. Grand mean of the estimated LFP within representative voxel during the pre- (red traces) and post- (blue traces) stimulus onset periods. Brodmann areas are indicated.

To evaluate the contribution of the transient and sustained responses to the frequency- and region-dependent patterns we have thus far observed, we also computed the RI for the time period from 500 to 1,000 ms poststimulus onset (always compared with the period 500–0 ms prestimulus onset period). Results are presented in Fig. 9 and show that the RI pattern is more lateralized in favor of the hemisphere contralateral to the simulation and that the contribution of frequencies above that of stimulation is highly reduced. This effect is particularly the case for the high gamma band and VFHOs within BAs 17 and 18.

DISCUSSION

This is the first study comparing results of fMRI analyses with LFPs estimated from scalp-recorded EEG and therefore in a completely noninvasive manner. Our methods allowed us to quantify correspondences between activation maps obtained

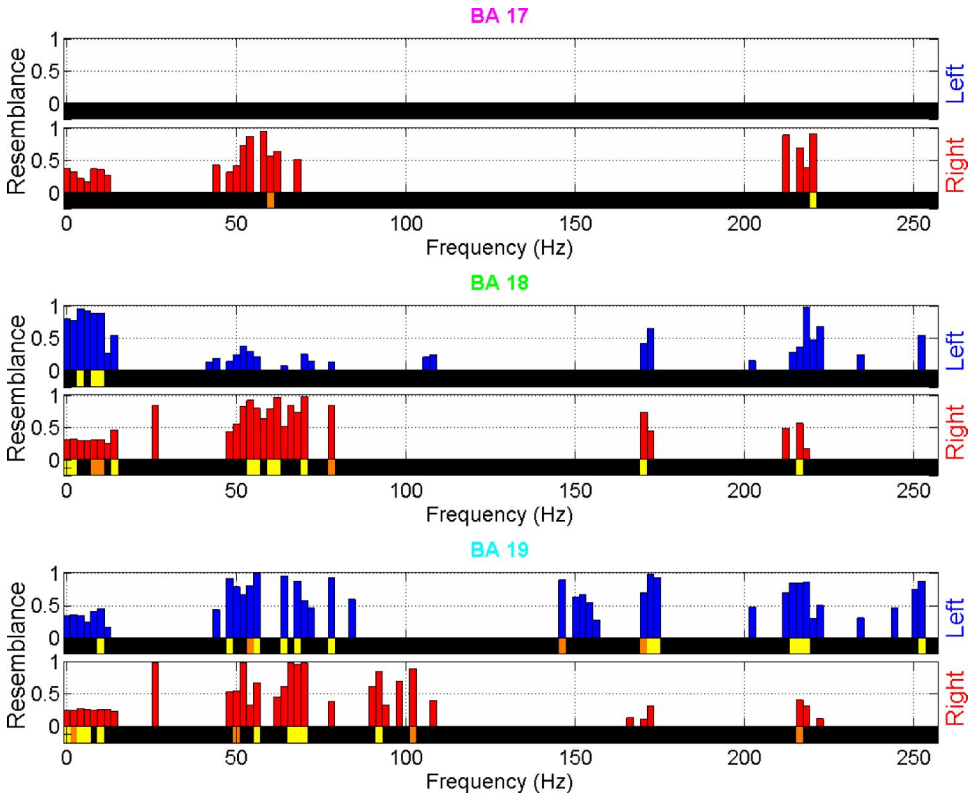

FIG. 6. Resemblance values between fMRI and LFP within BA17, BA18, and BA19 of the occipital lobe of each hemisphere. Blue bars represent the left hemisphere, and red bars the right. Below the bar plots, orange ($0.05<P<0.1$) and yellow ($P<0.05$) lines indicate the statistical significance of the resemblance value.

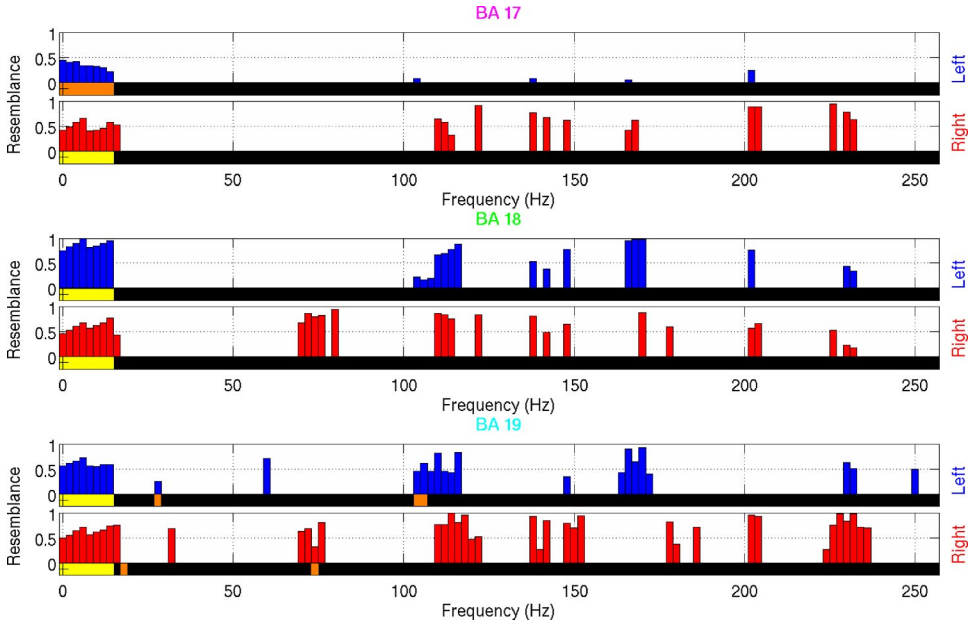

FIG. 7. Group analysis (2nd level of statistic) of the single *subject RI* computed with single subject results thresholded at $P < 0.001$ with a 3-voxel cluster threshold for both fMRI and estimated LFP (eLFP) analyses.

from stimulus-driven BOLD and EEG responses in healthy awake human subjects throughout the entire brain volume. We show that, following passive visual stimulation, this correspondence varies across regions and frequencies. We first discuss the methodological advances achieved in this study and then the neurophysiological implications of our results applying these methods.

The analyses developed here allow for the completely noninvasive and quantitative comparison of hemodynamic and electrophysiologic signals across the full range of frequencies and throughout the brain volume. The estimation of LFPs required the solution of the so-called bio-electromagnetic inverse problem, which is ill-posed due to its lack of a unique solution and will therefore vary in quality as a function of the a priori constraints one applies to obtain a unique solution. In our particular case, we used biophysically based constraints that differ considerably from purely mathematically based constraints and furthermore have several computational and empirical benefits (detailed in Grave de Peralta Menendez et al. 2004; see also Gonzalez Andino et al. 2005b; Gonzalez et al. 2006). Prior studies from our group evaluated the reliability of such an inverse solution in two manners. First, there have been

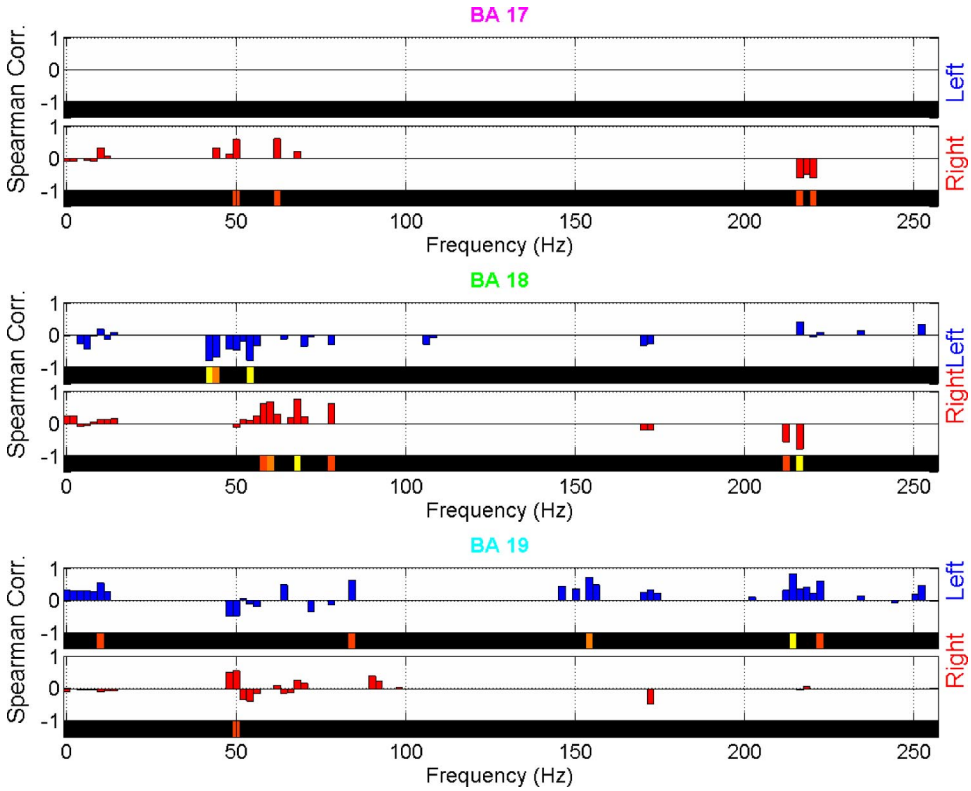

FIG. 8. Correlations between BOLD signal increase and eLFP power changes for each of the BAs of interest and for all the frequencies showing a nonzero RI. The colorbar indicates the significance of the sign test (yellow $P < 0.05$; orange $0.1 > P > 0.05$).

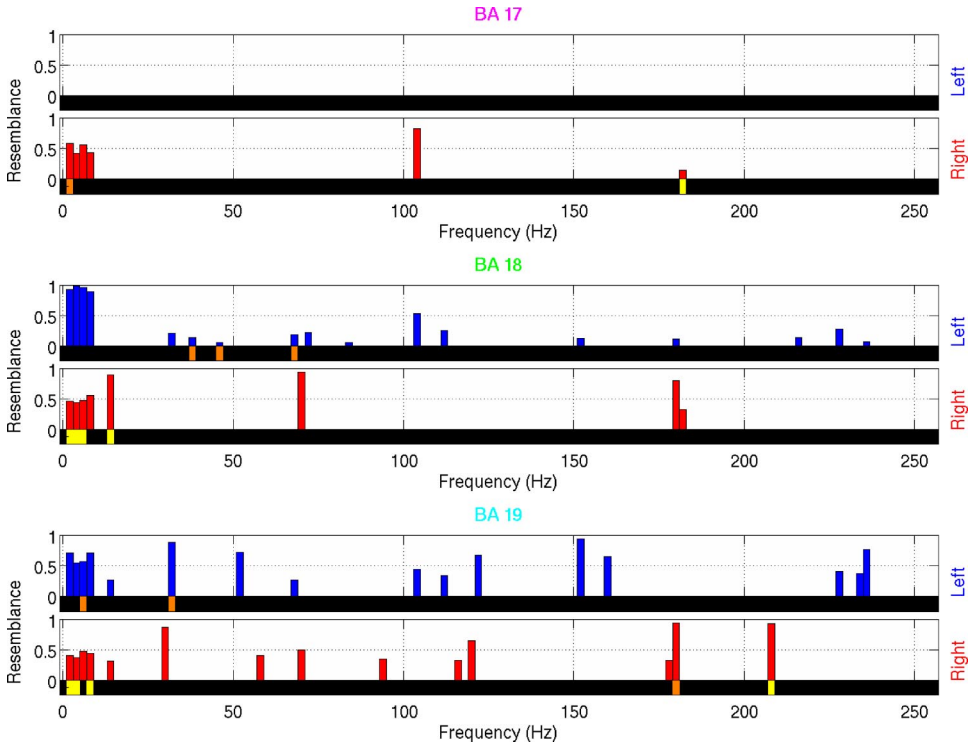

FIG. 9. Resemblance values between fMRI and LFP (in the 500- to 1,000-ms poststimulus onset period) within BA17, BA18, and BA19 of the occipital lobe of each hemisphere. Blue bars represent the left hemisphere, and red bars the right. Below the bar plots, orange ($0.05<P<0.1$) and yellow ($P<0.05$) lines indicate the statistical significance of the resemblance value.

comparisons between the localization of epileptic activity based on surface recordings and source estimations with the localization as determined by intracranial recordings during presurgical monitoring (e.g., Lantz et al. 2001; Michel et al. 1999, 2004). Second, empirical results from our group have demonstrated the correspondence between results from the ELECTRA inverse solution (i.e., that used in this study) and results from human fMRI and also monkey intracranial recordings (e.g., Grave de Peralta Menendez et al. 2004; Gonzalez Andino et al. 2005a; Murray et al. 2004, 2005a,b, 2006a,b). Despite such a good agreement between estimated and intracranial LFPs, the ELECTRA inverse solution cannot guarantee a perfect alignment of these signals. The existence of this small, but still not completely negligible, misalignment contributed to our decision to use a region—rather than a voxel-based metric. Here we focused our analyses on the measurement of stimulus-driven power changes because the absolute amplitude of the estimated potential at each brain voxel cannot be reliably quantified due to the ill-posed characteristic of inverse solutions (Grave de Peralta Menendez 1998). To preserve the contribution of high-frequency oscillations, we contrasted spectral power between the pre- and poststimulus onset periods. Assuming that the distribution of noise is independent of the timing of stimulus presentation, this method can detect power changes even where the noise is higher than the signal. Consequently, these methods can identify contributions from all frequencies (and not simply those with high signal amplitude at the scalp), demonstrating the utility of single-trial analysis in the study of brain electrical activity (e.g., Gonzalez Andino et al. 2005a,b). As it is the case for LFPs, the eLFPs do not offer information about spiking activity (discussed in more detail in the following text); however, we should note the increasing literature showing that the BOLD signal is better correlated with LFP than with spiking activity (e.g., Logothetis et al. 2001).

Quantitative comparisons between hemodynamic and electrophysiologic responses were obtained by introducing a new metric, *resemblance*, to evaluate the similarity between fMRI and single-frequency LFP activation maps within a certain region of interest. This metric was devised to accommodate voxel-level misalignment between fMRI and estimated LFPs, while also allowing for variation in neurovascular coupling across brain regions. Because fMRI data were acquired throughout the entire brain volume, it was equally essential to apply a distributed inverse solution that would not limit the calculation of *resemblance* to a set of predefined brain regions. An added advantage of using a distributed inverse solution is that it allowed for the generation of the empirical distributions used in our statistical analyses, which would not have been feasible had a fixed number of dipolar sources been assumed (i.e., activity at other, un-modeled brain locations would simply not have been estimated). Compared with previous attempts to integrate electrophysiologic and hemodynamic signals, this method allows analyses to be conducted throughout the brain with a fully noninvasive approach and without being spatially limited to the location of implanted electrodes, as is required for clinical evaluation and research (e.g., Mukamel et al. 2005).

In the present study, we applied these methods in the context of a passive visual stimulation paradigm. There were several bases for this choice. A passive protocol avoided contributions of task- and motor-related activity that might in turn influence activations within visual cortices (e.g., Martuzzi et al. 2006, 2007; van Atteveldt et al. 2007). We also opted here for a visual paradigm as these cortical regions (in particular primary visual cortex) are larger than their auditory counterparts and generally follow anatomical landmarks, making activity within them easier to disambiguate with both fMRI and EEG methods. For example, a stimulus restricted to a single visual quadrant results in a predictable spatial distribution of brain responses, given the known retinotopic functional organization

within the occipital lobe (e.g., Tootell et al. 1998). Finally, our choice was also based on the fact that the overwhelming majority of prior research has examined neurovascular coupling within visual cortices (Heeger et al. 2000; Kayser et al. 2004; Logothetis 2003; Logothetis et al. 2001; Makeig et al. 2002; Niessing et al. 2005; Rees et al. 2000). Such being said, it will be important for future studies to investigate *resemblance* with other stimuli/tasks and also within other sensory modalities.

While simultaneous recordings of EEG and fMRI have become increasingly prevalent (e.g., Debener et al. 2005, 2006, Eichele et al. 2005), it is worth reminding the reader of some limitations with such acquisitions with respect to the methods developed and applied here. For one, simultaneous acquisitions are currently limited in terms of the number of scalp electrodes used during recordings. As we were particularly interested in performing source estimations on single-trial and -subject data, it was particularly important to collect data from a high-density montage as required for an accurate estimation of intracranial sources (cf. Lantz et al. 2003). While systems are recently available for recordings with 96 or 128 channels, to our knowledge the technical issues regarding signal quality—in particular the distribution of noise across the electrode montage—have not yet been fully addressed (though will undoubtedly be resolved in the near future). The importance of this point is further highlighted when one considers data concerning the spatial accuracy of source estimations as a function of the number/distribution of scalp electrodes (Michel et al. 2004). Second (and in many ways more importantly), simultaneous EEG acquisitions within the MR scanner necessitate data filtering (typically with a low-pass $<$50 Hz) that would not have enabled us to investigate *resemblance* between high-frequency oscillations and the BOLD response. Furthermore, complications can arise during correction procedures for the balistocardiac artifact such that residual noise can persist in the data (see Mandelkow et al. 2007 for a recent discussion) that in turn can affect the quality of source estimations. Such being said, the method proposed in this paper can be employed irrespectively of whether EEG and fMRI data have been acquired in the same or in separate sessions provided that the aforementioned issues can be satisfactorily addressed to allow for reliable source estimations at a wide range of frequencies. Additionally, it will also undoubtedly be fruitful for future investigations to be conducted using simultaneous recordings wherein direct correlations of the same trials can be performed.

A parallel consideration with the present results concerns the possibility that separate EEG and fMRI sessions introduced state-dependent differences. Given that our analyses always contrasted prestimulus and poststimulus activity, we can assume that the general state of the participants remained reasonably constant throughout each session and that our statistical images (both fMRI and EEG) reflect stimulus-evoked responses. Any session-related differences would in principal likely only increase the likelihood of type II errors (i.e., of missing some relevant correlations), which we cannot unequivocally exclude.

We show that *resemblance* between fMRI activations and stimulus-driven spectral power changes in eLFPs was heterogeneous across frequencies. In particular, passive visual stimuli elicited changes within low frequencies ($\leq$14 Hz), the gamma band range (44–78 Hz), and VHFOs ($>$200 Hz). Other frequencies (e.g., 30 Hz) failed to elicit significant power changes in this study. The *resemblance* between low-frequency oscillations, which are the main contributors to the surface-recorded ERP, and fMRI activations is not altogether surprising. Numerous studies have reported spatial correspondence between ERP-based source estimations and fMRI results (e.g., Dale and Halgren 2001). Our results thus provide further evidence that the BOLD signal is coupled with eLFP as measured by ERPs.

Coupling between BOLD and eLFP is not limited to low frequencies. Indeed, high and significant *resemblance* was observed within the gamma band, consistent with previous animal studies that recorded from primary visual cortex (e.g., Kayser et al. 2004; Logothetis 2003; Logothetis et al. 2001; Niessing et al. 2005), and also within very high-frequency bands. This latter finding contrasts with the majority of findings in animals. This discrepancy might stem from the use of anesthetized preparations or the application of filters that prohibited the detection of effects at frequencies between 130 and 300 Hz (Logothetis et al. 2001; Niessing et al. 2005). It may also be related to the temporal window analyzed. Here, we focused our attention to the first 500 ms after stimulus onset, which is much shorter than the period analyzed by Kayser et al. (2004), who averaged the spectral information over a period extending from 200 to 12,000 ms poststimulus onset. One possibility, then, is that transient stimulus-related effects may play a more important role in our study than in Kayser et al. (2004), where sustained effects likely dominated. In fact, our analysis of the 500–1,000 ms poststimulus interval would indicate that patterns of RI vary between the 0–500 and 500–1,000 ms poststimulus intervals, likely reflecting differences between transient and sustained (steady-state) responses and their relationship to the BOLD signal. Further investigation is clearly required to determine the basis for this variation, including the application of time-frequency analyses to the methods developed here.

Although the origin and function of VHFOs remain to be detailed and are beyond the scope of the present study, it is worth noting that there is increasing evidence of the functional importance of VHFOs in animals (Chrobak and Buzsaki 1996; Grenier et al. 2001) with reports of stimulus-induced oscillations of $\leq$200 Hz within the visual cortex of awake, behaving cats (Siegel and Köenig 2003). In humans, VHFOs have been recorded noninvasively in response to somatosensory (Curio 2000; Miller et al. 2007) as well as visual stimuli (Gonzalez et al. 2006). The noninvasive study of VHFOs has typically been limited (and often obfuscated) by their small amplitude on the scalp, often below the noise level. Further application of the methods developed here will contribute to our understanding of the functional role of VHFOs in humans and their relationship to similar responses in animals. Such being said, our results provide a clear indication that the neurophysiologic origin of the BOLD signal is not limited to a single frequency band of the eLFP.

We also show that, following passive visual stimulation, *resemblance* between fMRI activations and stimulus-driven spectral power changes in eLFPs was heterogeneous across regions of the occipital lobe. Progression from lower to higher occipital visual areas (i.e., from BA17 to BA18 and to BA19) was mirrored by the observation of nonzero and significant *resemblance* values over progressively wider frequency ranges (Fig. 5). Additionally, nonzero and significant *resemblance*

values were initially restricted to the BA17 of the hemisphere contralateral to the stimulus but were then bilateral in BA18 and BA19. This heterogeneity could originate from differences in local neurovascular coupling and/or regional differences in the profile of neural responses to external stimuli (which might further vary as a function of task). Evidence that vascular density is more closely related to number of synapses rather than the number of neurons in an area (Logothetis and Wandell 2004) provides one measure of support that anatomical constraints may prove a stronger predictor of neurovascular coupling. Other studies, which did not directly compare BOLD and neural activity, provide evidence that different response frequencies subserve distinct functions within a given brain region (e.g., Fren and Ekhorn 2000; Fren et al. 2000; Fries et al. 2001; Siegel and König 2003; Kayser and König 2004), suggesting that the frequency of electrical activity is determined functionally rather than anatomically. While the present study constitutes an important first step, further improvements to these methods will be required to disambiguate the contribution of functional and anatomical variability in neurovascular coupling. This would undoubtedly also involve investigating other stimulus paradigms likely involving parametric modulation of stimulus features (e.g., contrast, retinotopic location, and flicker frequency) and sensory modalities, as well as the role of task demands. In parallel, it will be imperative for future studies in animals of the neural basis of the BOLD signal to be conducted in multiple brain regions beyond primary cortices, while also analyzing a fuller frequency range of LFP signals.

In summary, analyses of single-trial EEG across a wide range of frequencies, using noninvasively estimated intracranial LFPs, permitted the quantitative comparison of BOLD and LFP activation maps through the introduction of the metric *resemblance*. Our results show that fMRI and EEG signals are coupled at several frequency bands, including low frequencies that contribute to surface-recorded ERPs, gamma band, and VHFOs. Moreover, this coupling is heterogenous across frequencies and brain regions. The range of frequencies at which *resemblance* is observed may potentially be used as an additional means of characterizing functional hierarchies within the visual system. Our methods therefore open new directions for understanding the neurophysiological bases of brain-imaging data.

ACKNOWLEDGMENTS

We thank L. De Santis for assistance with EEG data collection.

GRANTS

This study has been supported by Swiss National Science Foundation Grants SNSF 3200B0-100606 and SNSF 3152A0-100745/1, the Center for Biomedical Imaging of Lausanne and Geneva, Switzerland (www.cibm.ch), and European Project FP6-IST-027140 (BACS, www.electrical-neuroimaging.ch).

REFERENCES

Blake R, Logothetis NK. Visual competition. *Nat Rev Neurosci* 3: 13–21, 2002.

Chrobak JJ, Buzsaki G. High-frequency oscillations in the output networks of the hippocampal-entorhinal axis of the freely behaving rat. *J Neurosci* 16: 3056–3066, 1996.

Curio G. Linking 600-Hz "spikelike" EEG/MEG wavelets ("sigma-bursts") to cellular substrates: concepts and caveats. *J Clin Neurophysiol* 17: 377–396, 2000.

Dale AM, Halgren E. Spatiotemporal mapping of brain activity by integration of multiple imaging modalities. *Curr Opin Neurobiol* 11: 202–208, 2001.

Debener S, Ullsperger M, Siegel M, Engel AK. Single-trial EEG-fMRI reveals the dynamics of cognitive function. *Trends Cogn Sci* 10: 558–563, 2006.

Debener S, Ullsperger M, Siegel M, Fiehler K, von Cramon DY, Engel AK. Trial-by-trial coupling of concurrent electroencephalogram and functional magnetic resonance imaging identifies the dynamics of performance monitoring. *J Neurosci* 25: 11730–11737, 2005.

Di Russo F, Pitzalis S, Aprile T, Spitoni G, Patria F, Stella A, Spinelli D, Hillyard SA. Spatiotemporal analysis of the cortical sources of the steady-state visual evoked potential. *Hum Brain Mapp* 28: 323–334, 2007.

Eichele T, Specht K, Moosmann M, Jongsma ML, Quiroga RQ, Nordby H, Hugdahl K. Assessing the spatiotemporal evolution of neuronal activation with single-trial event-related potentials and functional MRI. *Proc Natl Acad Sci USA* 102: 17798–177803, 2005.

Fren A, Eckhorn R. Functional coupling shows stronger stimulus dependency for fast oscillations than for low-frequency components in striate cortex of awake monkey. *Eur J Neurosci* 12: 1466–1478, 2000.

Fren A, Eckhorn R, Bauer R, Woelbern T, Gabriel A. Fast oscillations display sharper orientation tuning than slower components of the same recordings in striate cortex of the awake monkey. *Eur J Neurosci* 12: 1453–1465, 2000.

Fries P, Neuenschwander S, Engel AK, Goebel R, Singer W. Rapid feature selective neuronal synchronization through correlated latency shifting. *Nat Neurosci* 4: 194–200, 2001.

Friston KJ. Imaging neuroscience: principles or maps? *Proc Natl Acad Sci USA* 95: 796–802, 1998.

Gandhi SP, Heeger DJ, Boynton GM. Spatial attention affects brain activity in human primary visual cortex. *Proc Natl Acad Sci USA* 96: 3314–3319, 1999.

Gonzalez Andino SL, Michel CM, Thut G, Landis T, Grave de Peralta R. Prediction of response speed by anticipatory high-frequency (gamma band) oscillations in the human brain. *Hum Brain Mapp* 24: 50–58, 2005a.

Gonzalez Andino SL, Murray MM, Foxe JJ, Grave de Peralta Menendez R. How single-trial electrical neuroimaging contributes to multisensory research. *Exp Brain Res* 166: 298–304, 2005b.

Gonzalez SL, Grave de Peralta R, Thut G, Millan J del R, Morier P, Landis T. Very high frequency oscillations (VHFO) as a predictor of movement intentions. *Neuroimage* 32ö: 170–179, 2006.

Grave de Peralta Menendez R, Gonzalez-Andino SL. A critical analysis of linear inverse solutions to the neuroelectromagnetic inverse problem. *IEEE Trans Biomed Eng* 45: 440–448, 1998.

Grave de Peralta Menendez R, Gonzalez Andino SL, Morand S, Michel CM, Landis T. Imaging the electrical activity of the brain: ELECTRA. *Hum Brain Mapp* 9: 1–12, 2000.

Grave de Peralta Menendez R, Murray MM, Michel CM, Martuzzi R, Gonzalez Andino SL. Electrical neuroimaging based on biophysical constraints. *Neuroimage* 21: 527–539, 2004.

Grenier F, Timofeev I, Steriade M. Focal synchronization of ripples (80–200 Hz) in neocortex and their neuronal correlates. *J Neurophysiol* 86: 1884–1898, 2001.

Heeger DJ, Huk AC, Geisler WS, Albrecht DG. Spikes versus BOLD: what does neuroimaging tell us about neuronal activity? *Nat Neurosci* 3: 631–633, 2000.

Kayser C, Kim M, Ugurbil K, Kim DS, Konig P. A comparison of hemodynamic and neural responses in cat visual cortex using complex stimuli. *Cereb Cortex* 14: 881–891, 2004.

Kayser C, Köenig P. Stimulus locking and feature selectivity prevail in complementary frequency ranges of V1 local field potentials. *Eur J Neurosci* 19: 485–489, 2004.

Kreiman G, Hung CP, Kraskov A, Quiroga RQ, Poggio T, DiCarlo JJ. Object Selectivity of local field potentials and spikes in the macaque inferior temporal cortex. *Neuron* 49: 433–445, 2006.

Lantz G, Grave de Peralta Menendez R, Gonzalez Andino S, Michel CM. Noninvasive localization of electromagnetic epileptic activity. II. Demonstration of sublobar accuracy in patients with simultaneous surface and depth recordings. *Brain Topogr* 14: 139–147, 2001.

Lantz G, Grave de Peralta R, Spinelli L, Seeck M, Michel CM. Epileptic source localization with high density EEG: how many electrodes are needed? *Clin Neurophysiol* 114: 63–69, 2003.

Logothetis NK. The underpinnings of the BOLD functional magnetic resonance imaging signal. *J Neurosci* 23: 3963–3971, 2003.

Logothetis NK, Kayser C, Oeltermann A. In vivo measurement of cortical impedance spectrum in monkeys: implications for signal propagation. *Neuron* 55: 809–823, 2007.

Logothetis NK, Pauls J, Augath M, Trinath T, Oeltermann A. Neurophysiological investigation of the basis of the fMRI signal. *Nature* 412: 150–157, 2001.

Logothetis NK, Wandell BA. Interpreting the BOLD signal. *Annu Rev Physiol* 66: 735–769, 2004.

Makeig S, Westerfield M, Jung T-P, Enghoff S, Townsend J, Courchesne E, Sejnowski TJ. Dynamic brain sources of visual evoked responses. *Science* 295: 690–694, 2002.

Mandelkow H, Halder P, Brandeis D, Soellinger M, de Zanche N, Luechinger R, Boesiger P. Heart beats brain: the problem of detecting alpha waves by neuronal current imaging in joint EEG-MRI experiments. *Neuroimage* 37: 149–163, 2007.

Martuzzi R, Murray MM, Maeder PP, Fornari E, Thiran J, Clarke S, Michel CM, Meuli RA. Visuo-motor pathways in humans revealed by event-related fMRI. *Exp Brain Res* 170: 472–487, 2006.

Martuzzi R, Murray MM, Michel CM, Thiran JP, Maeder PP, Clarke S, Meuli RA. Multisensory interactions within human primary cortices revealed by BOLD dynamics. *Cereb Cortex* 17: 1672–1679, 2007.

Mathiesen C, Caesar K, Lauritzen M. Temporal coupling between neuronal activity and blood flow in rat cerebellar cortex as indicated by field potential analysis. *J Physiol* 523: 235–46, 2000.

Michel CM, Grave de Peralta R, Lantz G, Gonzalez Andino S, Spinelli L, Blanke O, Landis T, Seeck M. Spatiotemporal EEG analysis and distributed source estimation in presurgical epilepsy evaluation. *J Clin Neurophysiol* 16: 239–266, 1999.

Michel CM, Murray MM, Lantz G, Gonzalez S, Spinelli L, Grave de Peralta R. EEG source imaging. *Clin Neurophysiol* 115: 2195–2222, 2004.

Miller KJ, denNijs M, Shenoy P, Miller JW, Rao RPN, Ojemann JG. Real-time functional brain mapping using electrocorticography. *Neuroimage* 37: 504–507, 2007.

Mukamel R, Gelbard H, Arieli A, Hasson U, Fried I, Malach R. Coupling between neuronal firing, field potentials, and fMRI in human auditory cortex. *Science* 309: 951–954, 2005.

Murakami S, Hirose A, Okada YC. Contribution of ionic currents to magnetoencephalography (MEG) and electroencephalography (EEG) signals generated by guinea pig CA3 slices. *J Physiol* 553: 975–985, 2003.

Murakami S, Zhang T, Hirose A, Okada YC. Physiological origins of evoked magnetic fields and extracellular field potentials produced by the guinea pig CA3. *J Physiol* 544: 237–251, 2002.

Murray MM, Camen C, Gonzalez Andino SL, Bovet P, Clarke S. Rapid brain discrimination of sounds of objects. *J Neurosci* 26: 1293–1302, 2006a.

Murray MM, Foxe JJ, Wylie GR. The brain uses single-trial multisensory memories to discriminate without awareness. *Neuroimage* 27: 473–478, 2005a.

Murray MM, Imber ML, Javitt DC, Foxe JJ. Boundary completion is automatic and dissociable from shape discrimination. *J Neurosci* 26: 12043–12054, 2006b.

Murray MM, Michel CM, Grave de Peralta R, Ortigue S, Brunet D, Gonzalez Andino S, Schnider A. Rapid discrimination of visual and multisensory memories revealed by electrical neuroimaging. *Neuroimage* 21: 125–135, 2004.

Murray MM, Molholm S, Michel CM, Heslenfeld DJ, Ritter W, Javitt DC, Schroeder CE, Foxe JJ. Grabbing your ear: rapid auditory-somatosensory multisensory interactions in low-level sensory cortices are not constrained by stimulus alignment. *Cereb Cortex* 15: 963–974, 2005b.

Niessing J, Ebisch B, Schmidt KE, Niessing M, Singer W, Galuske RA. Hemodynamic signals correlate tightly with synchronized gamma oscillations. *Science* 309: 948–951, 2005.

Perrin F, Pernier J, Bertrand O, Giard MH, Echallier JF. Mapping of scalp potentials by surface spline interpolation. *Electroencephalogr Clin Neurophysiol* 66: 75–81, 1987.

Plonsey R. The nature of the sources of bioelectric and biomagnetic fields. *Biophys J* 39: 309–312, 1982.

Polonsky A, Blake R, Braun J, Heeger DJ. Neuronal activity in human primary visual cortex correlates with perception during binocular rivalry. *Nat Neurosci* 3: 1153–1159, 2000.

Rees G, Friston K, Koch C. A direct quantitative relationship between the functional properties of human and macaque V5. *Nat Neurosci* 3: 716–723, 2000.

Sibson NR, Dhankhar A, Mason GF, Rothman DL, Behar KL, Shulman RG. Stoichiometric coupling of brain glucose metabolism and glutamatergic neuronal activity. *Proc Natl Acad Sci USA* 95: 316–321, 1998.

Siegel M, Konig P. A functional gamma-band defined by stimulus-dependent synchronization in Area 18 of awake behaving cats. *J Neurosci* 23: 4251–4260, 2003.

Tallon-Baudry C, Bertrand O. Oscillatory gamma activity in humans and its role in object representation. *Trends Cogn Sci* 3: 151–162, 1999.

Thomson DJ. Spectrum estimation and harmonic analysis. *Proc IEEE* 70: 1055–1096, 1982.

Tootell RBH, Hadjikhani NK, Mendola JD, Marrett S, Dale AM. From retinotopy to recognition: fMRI in human visual cortex. *Trends Cogn Sci* 2: 174–183, 1998.

van Atteveldt NM, Formisano E, Goebel R, Blomert L. Top-down task effects overrule automatic multisensory responses to letter-sound pairs in auditory association cortex. *Neuroimage* 36: 1345–1360, 2007.

Worden MS, Foxe JJ. The dynamics of the spread of selective visual attention. *Proc Natl Acad Sci USA* 100: 11933–11935, 2003.